Title

Engineering the S-Layer of Caulobacter crescentus as a Foundation for Stable, High-Density, 2D Living Materials

Journal

ACS Synthetic Biology, 8(1)

ISSN

2161-5063

Authors

Charrier, Marimikel

Li, Dong

Mann, Victor R

et al.

Publication Date

2019-01-18

DOI

10.1021/acssynbio.8b00448

Peer reviewed

Engineering the S-layer of *Caulobacter crescentus* as a Foundation for Stable, High-Density, 2D Living Materials

Author List:

Marimikel Charrier[1], Dong Li[1], Victor R. Mann[1,2,†], Lisa Yun[1,†], Sneha Jani[1,†], Behzad Rad[1], Bruce E. Cohen[1], Paul D. Ashby[1,3], Kathleen R. Ryan[4,5], Caroline M. Ajo-Franklin[1,6,7*]

Author Affiliations: [1]Molecular Foundry, [3]Materials Sciences Division, [4]Environmental Genomics and Systems Biology Division, [6]Molecular Biophysics and Integrated Biosciences Division, and [7]Synthetic Biology Institute, Lawrence Berkeley National Laboratory, Berkeley, CA, 94720 [5]Department of Plant & Microbial Biology, [2]Department of Chemistry, University of California Berkeley, Berkeley, CA 94720

Corresponding author: Dr. Caroline Ajo-Franklin, 1 Cyclotron Rd, 67R5110, Berkeley, CA 94720, 510-486-4299, cajo-franklin@lbl.gov

Abstract

Materials synthesized by organisms, such as bones and wood, combine the ability to self-repair with remarkable mechanical properties. This multifunctionality arises from the presence of living cells within the material and hierarchical assembly of different components across nanometer to micron scales. While creating engineered analogs of these natural materials is of growing interest, our ability to hierarchically order materials using living cells largely relies on engineered 1D protein filaments. Here, we lay the foundations for bottom-up assembly of engineered living material composites in 2D along the cell body using a synthetic biology approach. We engineer the paracrystalline surface-layer (S-layer) of *Caulobacter crescentus* to display SpyTag peptides that form irreversible isopeptide bonds to SpyCatcher-modified proteins, nanocrystals, and biopolymers on the extracellular surface. Using flow cytometry and confocal microscopy, we show that attachment of these materials to the cell surface is uniform, specific, and covalent, and its density can be controlled based on the location of the insertion within the S-layer protein, RsaA. Moreover, we leverage the irreversible nature of this attachment to demonstrate via SDS-PAGE that the engineered S-layer can display a high density of materials, reaching 1 attachment site per 288 nm^2. Finally, we show that ligation of quantum dots to the cell surface does not impair cell viability and this composite material remains intact over a period of two weeks. Taken together, this work provides a platform for self-organization of soft and hard nanomaterials on a cell surface with precise control over 2D density, composition, and stability of the resulting composite, and is a key step towards building hierarchically ordered engineered living materials with emergent properties.

Keywords (up to 6):

RsaA, Engineered Living Materials, quantum dots, *Caulobacter*

Table of Contents Graphic:

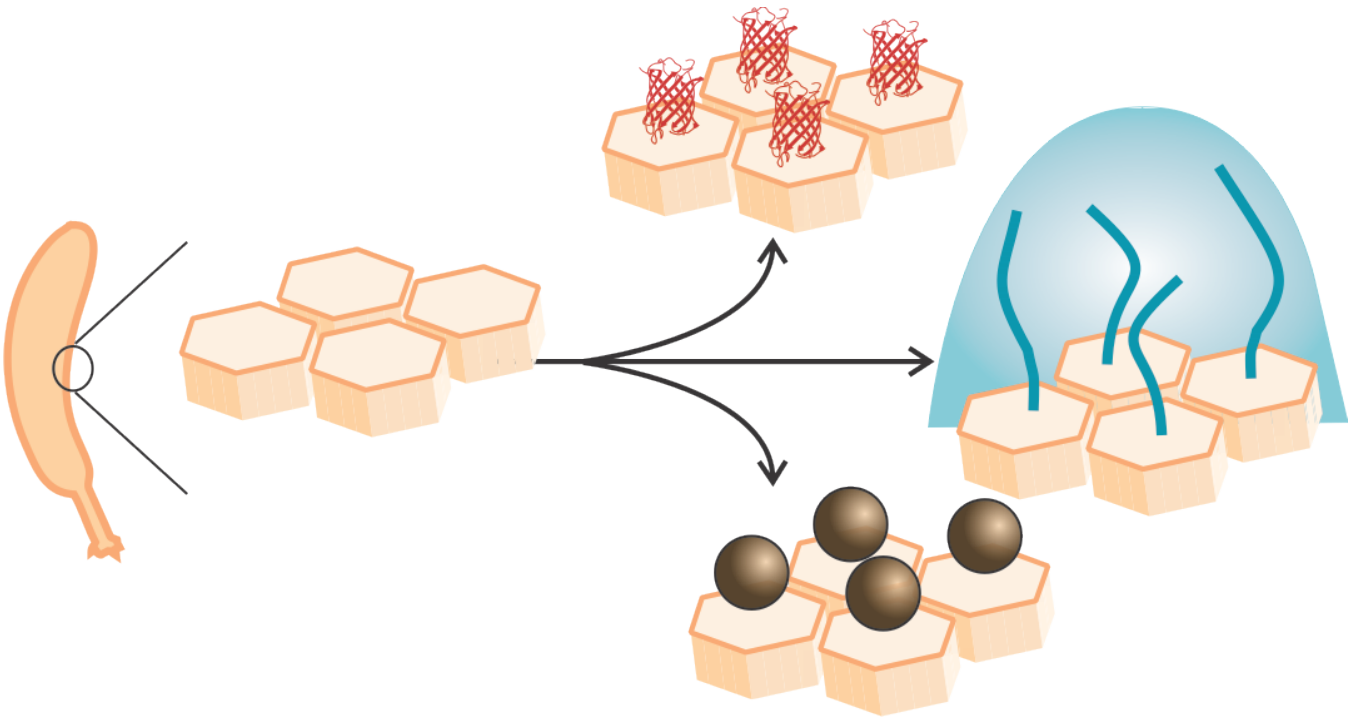

Living organisms hierarchically order soft and hard components to create biominerals that have multiple exceptional physical properties[1]. For example, the hierarchical structure of nacre creates its unusual combination of stiffness, toughness, and iridescence. Genetically manipulating living cells to arrange synthesized materials into engineered living materials (ELMs)[2,3] opens a variety of applications in bioelectronics[4], biosensing[5], smart materials[6], and catalysis[3-7]. Many of these approaches use surface display of 1D protein filaments[8–11] or membrane proteins[12,13] to arrange materials, while cell display methods that hierarchically order materials in 2D with controlled spatial positioning and density have yet to be fully developed. This gap limits the structural versatility and degree of control available to rationally engineer ELMs.

Surface-layer (S-layer) proteins offer an attractive platform to scaffold materials in 2D on living cells due to their dense, periodic structures, which form lattices on the outermost surface of many prokaryotes[14] and some eukaryotes[15]. These monomolecular arrays can have hexagonal (p3, p6)[16-17], oblique (p1, p2)[18-19], or tetragonal (p4)[20] geometries and play critical roles in cell structure[21-22], virulence[23], protection[24], adhesion[25], and more. Recombinant S-layer proteins can replace the wild-type lattice in native hosts, or can be isolated and recrystallized in vitro, on solid supports, or as vesicles[26]. These have been used for a number of applications[26, 27], including bioremediation[28] and therapeutics[29] on cells.

To date, only two S-layer proteins have solved atomic structures, allowing for sub-nanometer precise positioning of attached materials: SbsB of *Geobacillus stearothermophilus* PV72[18] and RsaA of *Caulobacter crescentus* CB15[30]. Of these two S-layer proteins, there is a well-established toolkit for the genetic modification of *C. crescentus*, as it has been studied extensively for its dimorphic cell cycle[31]. Additionally, *C. crescentus* is a Gram-negative, oligotrophic bacterium that thrives in low-nutrient conditions, and while a strict aerobe, can survive micro-aeration[32]. Together, this makes *C. crescentus* particularly suitable as an ELM chassis. RsaA forms a p6 hexameric lattice with a 22-nm unit cell (Figure 1a,b) at an estimated

density of 45,000 monomers per bacterium[33] and is amenable to peptide insertions[34]. Specific protein domains have been inserted in RsaA to bind lanthanide metal ions[35] or viruses[29]. However, engineered RsaA variants currently lack the ability to assemble a variety of materials, in an irreversible fashion, and with well-characterized density - all key features needed for ELMs.

Here we engineer RsaA as a modular docking point to ligate inorganic, polymeric, or biological materials to the cell surface of *C. crescentus* without disrupting cell viability. This 2D assembly system is specific, stable, and allows for control over the density of attached materials without the use of chemical cues, achieving a maximal coverage of ~25% of all possible sites, the highest density of cell-surface displayed proteins reported to our knowledge. This work forms the foundation for a new generation of hierarchically assembled ELMs.

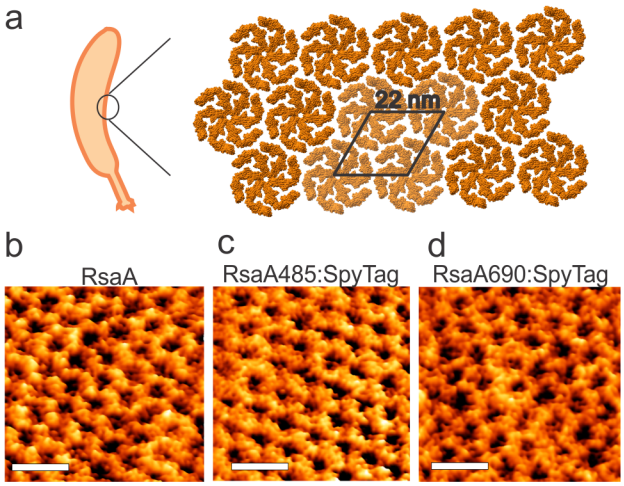

Figure 1: RsaA forms a 2D hexameric lattice on the surface of *C. crescentus*. (a) Structure of the RsaA lattice.[30] (b) High resolution AFM images of the wild-type RsaA lattice (strain MFm111), (c) RsaA485:SpyTag (strain MFm 118), (d) RsaA690:SpyTag (strain MFm 120) on the surface of *C. crescentus* cells. In all three cases, a well-ordered, hexagonal protein lattice is observed. The unit cell length (center-to-center distance between adjacent hexagons) is 22 ± 1nm, which is the same as reported in literature. Scale bar is 40nm. See Methods for experimental details of AFM.

Results and Discussion

Design and Construction of Caulobacter crescentus *S-layer variants for surface display*

To display materials on the surface of *C. crescentus* cells, we designed a genetic module that meets four criteria: (i) a solution-exposed peptide that drives (ii) specific, stable, and stoichiometric attachment (iii) with tunable occupancy and (iv) that does not disrupt RsaA coverage. We hypothesized that varying the location of the binding peptide within RsaA might affect its solution accessibility leading to strains that have a range of occupancy. Therefore, we selected a panel of locations arrayed across the entire RsaA monomer (Figure 2a) to insert the peptide. Smit and colleagues previously identified two sites, at amino acid positions 723 and 944, that allowed for surface display of peptides[34], so we started with these positions. We then selected six additional sites that are known to be susceptible to proteolytic cleavage, presumably by the previously characterized S-layer Associated Protease (sapA)[36]. We hypothesized these additional sites, immediately following amino acid positions 277, 353, 467, 485, 622, and 690, might be accessible in a *ΔsapA* strain which we created (abbreviated as

CB15N*ΔsapA*). All subsequent engineering to the eight positions within *rsaA* was done in this background.

To achieve specific, stoichiometric, and irreversible conjugation to RsaA, we employed the split-protein system SpyTag-SpyCatcher[37,38], which forms an isopeptide bond between the SpyCatcher protein and SpyTag peptide. The RsaA S-layer can accommodate insertion of large peptide sequences[29,35], which suggested that the 45-mer SpyTag peptide sequence, flanked on each side by a $(GSSG)_4$ flexible linker for accessibility, may be integrated and displayed without disrupting S-layer assembly. This modified lattice should then allow the formation of a covalent isopeptide bond between any material displaying the SpyCatcher partner protein and the SpyTag on the cell surface.

Since expression of RsaA from a p4-based plasmid in an *ΔrsaA* background formed a lattice structure indistinguishable from genomically-expressed RsaA (Figure 1b, we initially constructed p4-based plasmids[39] that constitutively express RsaA-SpyTag fusions (Table S2) and transformed them into *C. crescentus* JS4038[39]. Examination of the cell surface of two of these plasmid-bearing strains by AFM confirmed that RsaA-SpyTag was expressed and showed that the RsaA-SpyTag formed a S-layer lattice with the same nanoscale ordering as wild-type RsaA (Figure 1b-d). However, we observed significant growth defects, morphological changes, and unstable RsaA expression in all of the plasmid-bearing strains (Figure S1). For this reason, we integrated SpyTag and its linkers directly into the genomic copy of *rsaA* (Figure 2b) in the CB15N*ΔsapA* background (Table S1). We notate these strains based on the SpyTag insertion site, e.g. *rsaA*690:SpyTag denotes insertion of the SpyTag and $(GSSG)_4$ linkers immediately after amino acid 690. No growth defects or morphological changes are apparent in any of the engineered strains, implying that our genomic insertions do not affect cell viability, and therefore these strains were used for the rest of the study. These observations suggest the more regulated genomic expression of recombinant *rsaA*, a highly-transcribed gene, sidesteps growth impairments.

SDS-PAGE analysis of RsaA-SpyTag expression of wild-type (CB15NΔ*sapA*) and engineered cells (*rsaA*:SpyTag variants) shows the expected band for wild-type RsaA at 110 kDa (Figure 2c), in line with the observed migration of RsaA on SDS-PAGE[40,30]. Moreover, all eight engineered proteins have comparable expression levels to wild-type RsaA and show the small increase in molecular weight associated with SpyTag and its linkers (Figure 2c). These observations demonstrate that successful expression of SpyTag within RsaA at a range of different positions does not adversely affect RsaA expression levels.

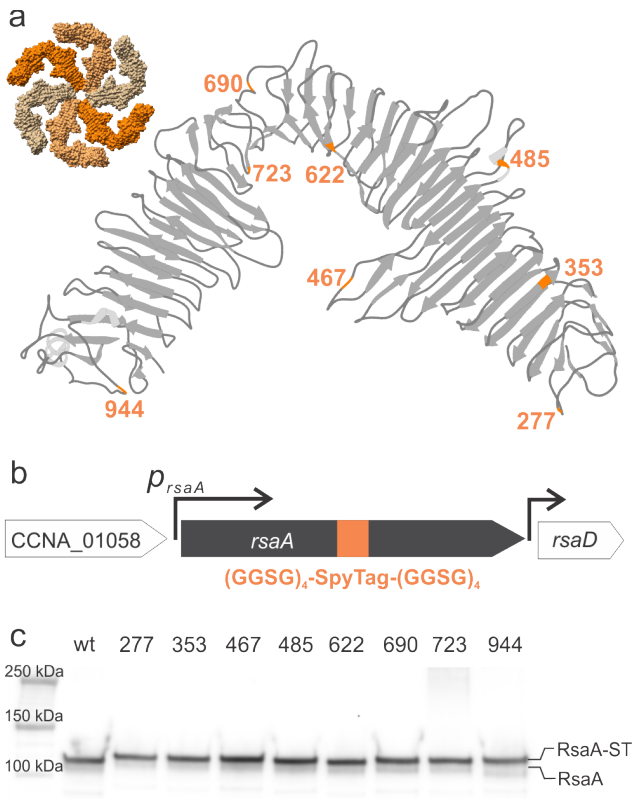

Figure 2: Design and expression of RsaA-SpyTag in *C. crescentus*. a) Ribbon diagram of the RsaA monomer structure[30] indicating SpyTag insertion sites (orange). Inset shows a space-filling model of the RsaA hexamer. b) Design of engineered *C. crescentus* strains expressing RsaA-SpyTag. SpyTag flanked by upstream and downstream $(GGSG)_4$ spacers was directly inserted into the genomic copy of *rsaA*. c) Immunoblot with anti-RsaA antibodies of *C. crescentus* strains whole cell lysate. The band corresponding to RsaA increases in molecular weight from wild-type RsaA (lane 2) to RsaA-SpyTag at the each insertion sites (lanes 3-10).

Engineered S-layers specifically display proteins ligated to the cell surface

To explore accessibility of the SpyTag peptide on the *C. crescentus* cell surface, we engineered and purified a fusion of SpyCatcher and mRFP1[41,42,43]. We incubated the wild-type

and engineered *rsaA*690:SpyTag strains with the fluorescent SpyCatcher-mRFP1 protein or mRFP1 alone, washed away unbound protein, and visualized mRFP1 attachment to individual cells via confocal microscopy (Figure 3). No significant mRFP1 fluorescence is apparent in controls that used *C. crescentus* expressing wild-type RsaA or mRFP1 without SpyCatcher (Figure 3 a-c), indicating no significant non-specific binding of mRFP1 to the cell surface. When SpyTag is displayed on RsaA and SpyCatcher-mRFP1 is present, bright and uniform fluorescence is observed along the morphologically-normal, curved cell surface, including the stalk which is covered by the S-layer lattice[17,30,33] (Figure 3d). These observations indicate engineering SpyTag into RsaA enables specific binding of a SpyCatcher fusion protein to the extracellular surface, and furthermore illustrates that engineering SpyTag into the S-layer does not substantially affect the morphology of *C. crescentus*.

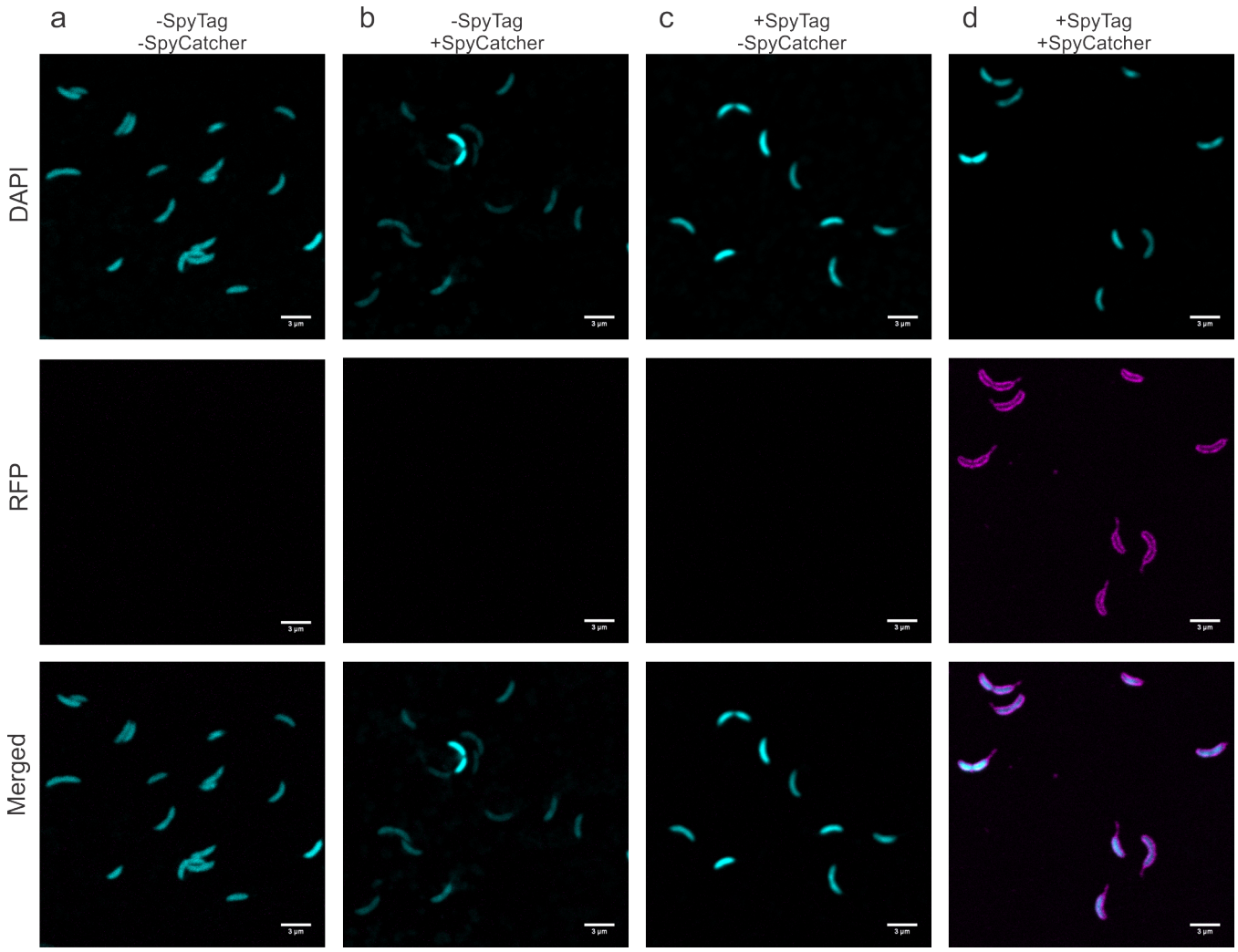

Figure 3: SpyCatcher protein fusions ligate specifically to the surface of *C. crescentus* expressing RsaA-SpyTag. a-d) Confocal fluorescence images of *C. crescentus* cells visualized in DAPI and RFP channels. Cells expressing wild-type RsaA incubated with a) mRFP1 or b) SpyCatcher-mRFP1. Cells expressing RsaA690-SpyTag with c) mRFP1 or d) SpyCatcher-mRFP1. Only when the SpyCatcher-mRFP1 probe is introduced to cells displaying SpyTag (d) is RFP fluorescence tightly associated with the cell membrane observed, including the stalk region. Scale bar = 3μm.

Density of attached materials is controlled by insertion location

Having demonstrated specific display of proteins on the surface, we turned to the hypothesis that the solution-accessibility of the eight insertion locations within the RsaA monomer would allow us to vary the density of attached materials. To quantify this relative accessibility, we again incubated the engineered strains with SpyCatcher-mRFP1, washed away unbound protein, and measured the fluorescence intensity per cell with flow cytometry.

176 The engineered strains show a >100-fold increase in fluorescent signal (Figure 4a) over the
177 wild-type control, indicating that all eight positions can ligate significant amounts of SpyCatcher
178 fusion protein. Among the eight engineered strains, there is a ~5-fold variation in the levels of
179 ligation (Table 1), with *rsaA*467:SpyTag and *rsaA*485:SpyTag showing the highest and lowest
180 densities of binding, respectively. These results unveil six new permissive insertion sites within
181 RsaA and show that the amount of protein bound to the cell surface can be controlled by
182 utilizing these different insertion points.

183 To test that the fusion protein is irreversibly conjugated to RsaA-SpyTag, we incubated
184 strain *rsaA*467:SpyTag, which showed the highest fluorescence by flow cytometry, with
185 SpyCatcher-mRFP1, boiled the sample for 10 minutes with SDS and 2-mercaptoethanol, and
186 visualized covalent attachment by SDS-PAGE (Figure 4b). The band corresponding to RsaA-
187 SpyTag (Figure 4b) decreases in intensity while the band corresponding to the RsaA-SpyTag-
188 SpyCatcher-mRFP1 assembly appears in as little as 1 hour and increases over 24 hours.
189 Subsequent immunoblotting of this reaction with anti-RsaA polyclonal antibodies confirms that
190 the assembly band contains RsaA (Figure S2). These observations indicate the binding is
191 covalent.

192 We leveraged the formation of this covalent bond to quantify the absolute density of
193 SpyCatcher-mRFP1 displayed on the *C. crescentus* cell surface. The density of the RsaA band
194 decreases by 23 ± 5% (n = 6, refer to Methods for the details of this calculation), indicating that
195 nearly a quarter of the *rsaA*467:SpyTag protein is ligated to SpyCatcher-mRFP1 after 24 hours.
196 Based on the estimate of 45,000 RsaA monomers per cell[33], this translates to >11,000 copies of
197 SpyCatcher-RFP displayed on the cell surface, an average density of 1.5 SpyCatcher-RFPs per
198 RsaA hexamer, or 1 SpyCatcher-RFP per 288 nm^2. Combining this information with the flow
199 cytometry data, we calculated the percentage of the RsaA lattice that is covalently modified can
200 be controlled over a range from 4-23% by varying the engineered location (Table 1, refer to
201 Methods for the details of this calculation). These results provide quantitative information on

how to utilize position-dependent insertion of SpyTag in RsaA to tune the density of attached materials and thus substantially improve our ability to rational engineer ELMs.

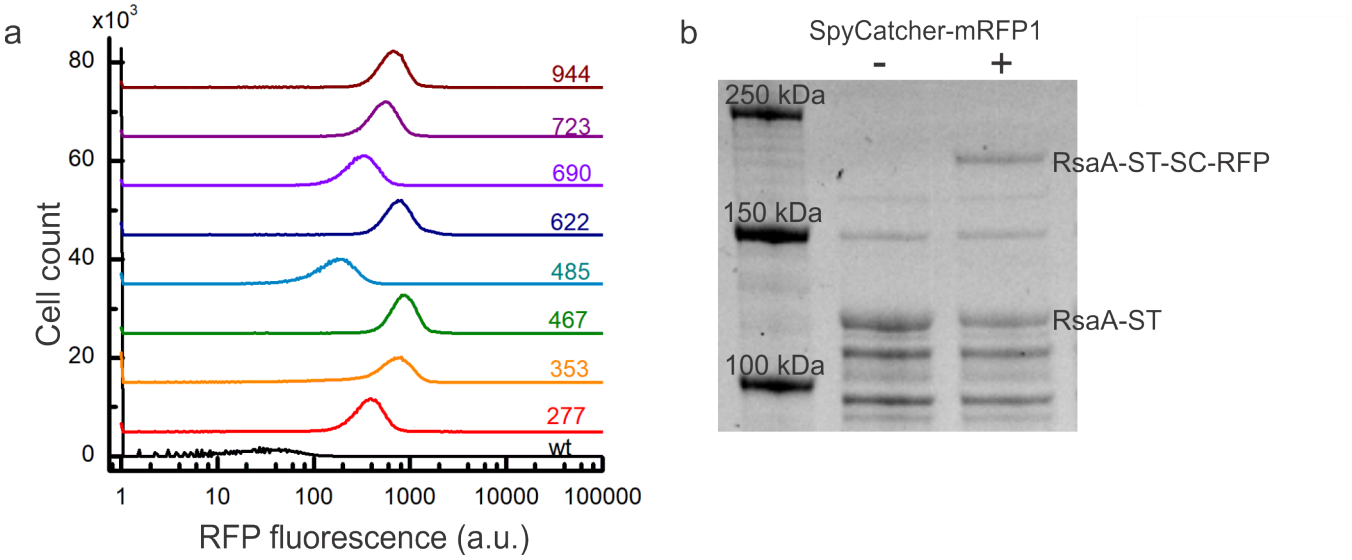

Figure 4: SpyCatcher protein fusions covalently bind to RsaA-SpyTag with variable occupancy according to the SpyTag location. a) Flow cytometry histograms of RFP fluorescence per cell for strains expressing wild-type RsaA (black) and RsaA-SpyTag (colored lines) incubated with SpyCatcher-mRFP1 for 1 hour. Baselines are offset for clarity. All eight strains displaying RsaA-SpyTag show an increase in the intensity of RFP fluorescence over the negative control with their intensity varying based on where SpyTag is inserted within RsaA. b) SDS-PAGE of whole cell lysates from the *rsaA*467:SpyTag strain incubated for 24 hours without (lane 2) and with (lane 3) SpyCatcher-mRFP1 protein. Appearance of a higher molecular weight band only in the reaction containing SpyCatcher-mRFP1 indicates covalent binding to RsaA-SpyTag.

Table 1. Normalized and absolute levels of SpyCatcher-mRFP1 ligation.

Location of SpyTag insertion	Absolute intensity of bound SpyCatcher-mRFP1, I_{loc} (Mean ± SEM)	Relative SpyCatcher-mRFP1 binding, $I_{loc,\,rel}$ (Mean ± SEM)	Percentage of RsaA-SpyTag covalently modified (%), P_{loc} (Percentage, SEM)
277	$373.9 \pm 3.6\times10^{-01}$	$0.43 \pm 5.5\times10^{-04}$	9.9 ± 2.4
353	$606.8 \pm 8.5\times10^{-01}$	$0.70 \pm 1.1\times10^{-03}$	16.0 ± 4.9
467	$871.6 \pm 7.3\times10^{-01}$	$1.00 \pm 1.2\times10^{-03}$	23.0 ± 2.0
485	$170.3 \pm 2.3\times10^{-01}$	$0.20 \pm 3.2\times10^{-04}$	4.5 ± 1.3
622	$778.1 \pm 8.6\times10^{-01}$	$0.89 \pm 1.2\times10^{-03}$	20.5 ± 5.4
690	$316.3 \pm 3.3\times10^{-01}$	$0.36 \pm 4.9\times10^{-04}$	8.3 ± 2.1
723	$536.0 \pm 4.8\times10^{-01}$	$0.61 \pm 7.5\times10^{-04}$	14.1 ± 3.3
944	$668.9 \pm 6.1\times10^{-01}$	$0.77 \pm 9.6\times10^{-04}$	17.6 ± 4.2

Arraying hard and soft materials on the surface of engineered cells

Next we sought to test whether engineered RsaA could assemble soft materials on the surface of *C. crescentus*. We selected elastin-like polypeptide (ELP) as our model soft material because it is well-studied, easily expressed recombinantly, and exhibits interesting temperature-dependent phase behavior[44]. We incubated a SpyCatcher-ELP-mCherry fusion protein[45] with the wild-type and *rsaA*690:SpyTag strains, washed away unbound protein, and imaged individual cells by confocal microscopy. As before, we observe no significant mCherry fluorescence from incubations lacking either SpyTag or SpyCatcher (Figure 5a,b), indicating there is no significant non-specific binding of ELP-mCherry to the *C. crescentus* surface. When both SpyTag and SpyCatcher are present, we observe significant mCherry fluorescence that uniformly covers the cell surface (Figure 5c). This work indicates that the engineered RsaA lattice can assemble polymeric materials to the cell surface (Figure 5).

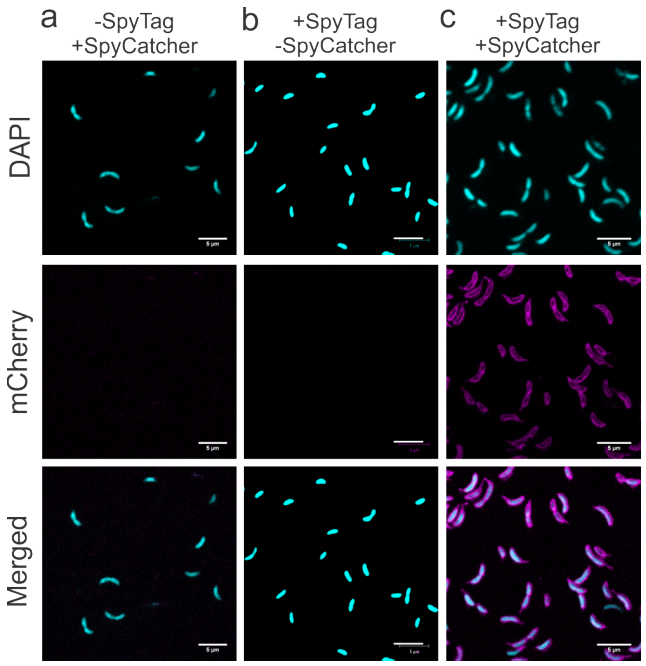

Figure 5: Engineered RsaA assembles biopolymers on the *C. crescentus* cell surface. a-c) Confocal fluorescence images of *C. crescentus* cells incubated with ELP-mCherry fusion proteins visualized in DAPI and mCherry channels. Cells expressing a) wild-type RsaA incubated with SpyCatcher-ELP-mCherry and b) expressing RsaA690:SpyTag incubated with ELP-mCherry. Only the *rsaA*690:SpyTag strain incubated with SpyCatcher-ELP-mCherry (c) shows signal along the cell membrane in the mCherry channel, indicating specific assembly on the cell surface. Scale bar = 5μm.

To explore the diversity of structures that can be created at the cell surface using SpyCatcher-SpyTag ligation, we tested the capacity of engineered bacteria to conjugate CdSe/ZnS semiconductor quantum dots (QDs)[46,47]. SpyCatcher-functionalized QDs were generated through attachment of a heterobifunctional PEG linker molecule to an amphiphilic polymer encapsulating the QD surface. Subsequent incubation with SpyCatcher-Ser35Cys single cysteine mutant protein yielded QDs with surface-displayed SpyCatcher protein. We incubated PEGylated QDs and SpyCatcher-conjugated QDs (see Supporting Information) with wild-type and *rsaA*690:SpyTag strains, performed a wash, and visualized individual cells via confocal microscopy. There is significant QD fluorescence along the cell body in samples containing SpyCatcher-QDs and the engineered strain, while there is no significant fluorescence with the wild-type strain (Figure 6) or the PEGylated QDs. This demonstrates that hard nanomaterials can also be specifically attached to the engineered RsaA lattice.

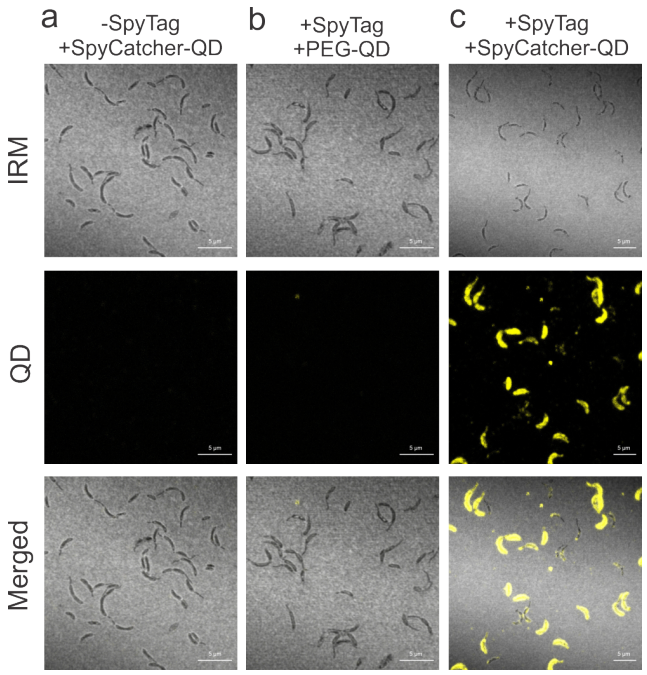

Figure 6: Engineered RsaA assembles inorganic nanocrystals on the *C. crescentus* cell surface. a-c) IRM and confocal fluorescence images of *C. crescentus* cells incubated with QDs. Cells expressing a) wild-type RsaA incubated with SpyCatcher-QDs and b) expressing RsaA690:SpyTag incubated with PEG-QDs. c) Cells expressing RsaA690:SpyTag incubated with SpyCatcher-QDs show QD fluorescence along the cell surface, indicating specific assembly of SpyCatcher-QDs by the engineered strain. Scale bar = 5μm.

Nanoparticle attachment does not affect cell viability

Finally, we explored the effect of coating the surface of the *C. crescentus* cells with nanoparticles on their viability, as this is key to creating hybrid living materials that remain metabolically active over time[48]. We incubated control wild-type (CB15NΔ*sapA*) and engineered *rsaA*467:SpyTag cells with or without SpyCatcher-QDs for two weeks, sampled the cultures periodically, and enumerated the living cells (CFU/mL). We also imaged the samples using confocal microscopy to determine whether the SpyCatcher-QDs remained stably bound to the engineered S-layer. Under all conditions, the total cell numbers decrease over the two week duration, which is expected since nutrients are not replenished (Figure 7a). More importantly, the number of viable cells in the wild-type culture without QDs is not significantly different from the wild-type with unbound SpyCatcher-QDs, the *rsaA*467:SpyTag culture without QDs, or the *rsaA*467:SpyTag culture with QDs (Figure 7a). These results indicate that neither unbound

SpyCatcher-QDs in the wild-type culture nor surface-bound SpyCatcher-QDs on the engineered cells affect viability, and there is no notable difference in viability between the wild-type and engineered cells. One possible interpretation of this cell viability is that the S-layer acts as an effective barrier, preventing disruption of the outer cell membrane, fulfilling one of its key evolutionary roles[49–51]. Imaging reveals that SpyCatcher-QDs remain attached to the cell surface over two weeks (Figure 7B) and non-specific binding of SpyCatcher-QDs on the surface of wild-type cells is not observed (Figure S5), once again highlighting the specificity and stability of the SpyTag-SpyCatcher system on S-layers. We do note that QD emission decreases over the course of the experiment, which may be due to non-specific cleavage of bonds between RsaA and the QD, turnover of the RsaA protein, or slow QD quenching in biological media. SpyCatcher-QDs incubated alone in M2G buffer show a ca. 30% decrease in emission over 14 days (Figure S6), which suggests QD quenching is the likely cause of observed emission decrease in QD-RsaA conjugates. Nonetheless, these results demonstrate that engineered RsaA can be used to generate stable living materials that require cells to remain viable for extended periods of time.

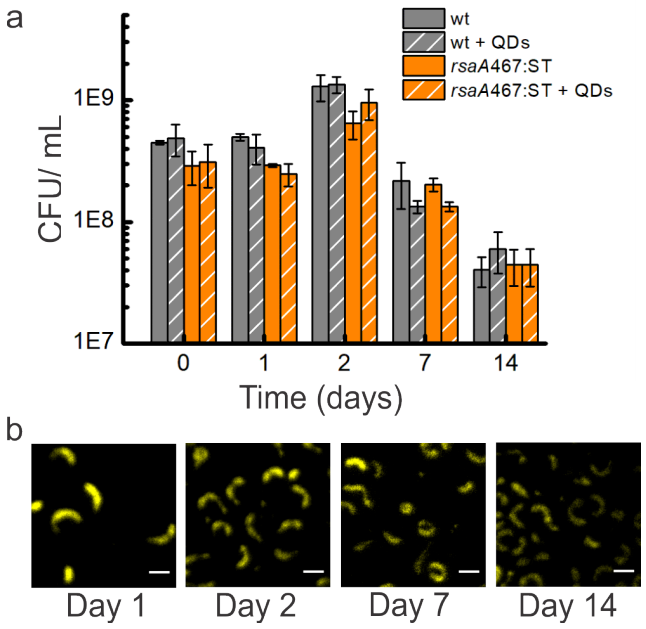

Figure 7: Engineered *C. crescentus* with ligated SpyCatcher-QDs remain viable over two weeks. a) Viability of CB15NΔ*sapA* (wild-type) and CB15NΔ*sapA rsaA*467:SpyTag strains incubated without or with SpyCatcher-QDs (+ SC-QD) was assessed by quantifying colony forming units/mL (CFU/mL) as described in the Methods section. Data shown represent mean ± standard deviation of three replicates per condition. The CFU/mL of cells with SC-QDs is very similar to that of cells grown without SC-QDs. b) Confocal images of r*saA*467:Spytag + SC-QD show QD fluorescence over the two week duration indicating sustained attachment of SpyCatcher-QDs to the engineered strain. Scale bar = 3μm.

Advancement of RsaA S-layer as a platform for controlled material assembly

In summary, we show that the S-layer of *C. crescentus*, RsaA, is a versatile platform for cell surface attachment of proteins, biopolymers, and inorganic materials when combined with the Spy conjugation system. We demonstrate that eight sites are available for peptide insertion within RsaA and that the insertion location tunes the attachment density. Ligation to the RsaA-SpyTag lattice is highly specific and covalent, with the absolute level of density of RsaA-displayed proteins reaching ~25% of the total RsaA, or 1 site per 288 nm^2, which is the highest density of cell-surface displayed proteins reported to our knowledge. Moreover, we show that QD-*C. crescentus* composites assembled via RsaA-SpyTag form engineered living materials that persist for at least two weeks. In the following, we discuss possible reasons for the site-dependent variation in attachment density, specific applications for cell-display using the RsaA platform, and the broader opportunities it opens in the area of ELMs.

We observed that the relative ligation efficiency varies ~5-fold across the eight permissive sites, with *rsaA*467:SpyTag affording the densest array of SpyCatcher-mRFP1. This variance is not due to protein expression levels, which do not vary significantly between strains (Figure 2c), and is unlikely to be caused by disruption to the S-layer lattice as our findings indicate that SpyTag insertions to not alter the structure on the nanometer scale (Figure 1b-d) but may be due to solvent-accessibility within the RsaA, steric clashes between sites on nearby RsaA monomers, or a combination of these factors. The most efficient binding site, RsaA467:SpyTag, is in an unstructured loop in a gap in the hexamer (Figure 2a), potentially giving more freedom for the SpyTag peptide to access a SpyCatcher-fusion. Since

RsaA485:SpyTag and RsaA690:SpyTag are in an alpha-helix and a calcium-binding pocket, respectively (Figure 2a), these insertions could be causing local disruption in structure, leading to the lower occupancy we observe (Table 1). Additionally, position 277 is located near the pore of the hexamer, resulting in the five neighboring positions being between 1.4 and 2.8 nm away. Since the entire engineered linkage to mRFP1, i.e. $(GSSG)_4$-SpyTag-SpyCatcher-mRFP1, is roughly 2.9 by 2.5 by 15 nm in dimensions, it is likely that some of the neighboring sites are sterically inaccessible once a single mRFP1 is bound. Further investigation will be required to untangle these possibilities.

Engineered C. crescentus *opens new possibilities for hierarchical assembly of hybrid living materials*

The engineered S-layer system described here offers immediate opportunities for engineering enzyme cascades on cells and encapsulation in hydrogels. By eliminating the need for direct fusion of enzymes to the S-layer, we avoid potential enzyme activity inhibition caused by expressing the protein in tandem with the S-layer monomer[52]. In addition, the varied ligation density and SpyTag spatial positioning engineered in our strains provides flexibility to attach enzymes in the most ideal pattern. As another potential application, bacterial cells are frequently encapsulated in hydrogels to enhance their stability as probiotics[53], as adjuvants to plant growth in agriculture[54], or as biostimulants in wastewater treatment[55]. Typically no specific adherence mechanism is engineered between bacterial cells and the hydrogel, and many factors can affect gel stiffness[56], including number or type of cells and media content. By using direct attachments between the S-layer and hydrogel polymers, we may achieve more stability and unique mechanical properties due to the sheer number of covalent crosslinks the between the engineered S-layer and the hydrogel matrix.

Our work more broadly introduces several foundational aspects useful for engineering ELMs. First, our results (Figure 3, 5, 6) suggest any material on which SpyCatcher can be

conjugated can be self-assembled on the modified 2D S-layer lattice, thus avoiding the labor-intensive reengineering of RsaA with peptides designed for specific targets. This makes our strain a versatile starting point for building an array of ELMs. Second, while ELMs with impressive functionality have been assembled via 1D curli fiber proteins and the type III secretion apparatus[57], the 2D structure of the S-layer lattice yields another dimension of spatial control. Because hierarchical ordering underlies the exceptional physical properties of many natural biocomposites, the ability to regulate spacing of different components in multiple dimensions is key to rationally designing predictable ELMs. Third, we can attach materials densely to the cell surface; here we demonstrate ligation of ~11,000 copies of a protein to the *C. crescentus* cell surface, or 1 attached protein per 288 nm^2. This is the highest density of surface arrayed proteins reported in a bacterium to our knowledge. Being able to access high densities is important because it ensures well-ordered structures while the ability to tune density may result in control over material properties. Lastly, the combined robustness of the covalent SpyCatcher-SpyTag system, the RsaA S-layer, and *C. crescentus* enables long-term persistence of the assembled structure and cell viability in an ELM even under low aeration and nutrient conditions. We envision this robustness will enable ELMs that can function in nutrient-poor environments with minimal intervention. Thus, the RsaA platform described here offers a modular, stable platform for assembling materials densely in 2D that opens new possibilities for constructing ELMs.

Conclusions

In closing, hierarchically ordered hybrid materials could allow for the rational design of materials with the emergent properties seen in natural materials. A bottom-up approach towards these engineered living materials is controlled attachment of materials to the cell surface in 2D, which we achieved by engineering the *C. crescentus* S-layer with the Spy conjugation system

for specific attachment of hard, soft, and biological materials at controllable densities. This modular base could lead to higher ordered materials that combine the functions of inorganic materials with the self-assembly and self-healing properties of living cells for applications that span medicine, infrastructure, and devices.

Methods

Strains:

All strains used in this study are listed in Table S1. *C. crescentus* strains were grown in PYE media at 30°C with aeration. *E. coli* strains were grown in LB media at 37°C with aeration. When required, antibiotics were included at the following concentrations: For *E. coli*, 50μg/ml ampicillin, 20μg/ml chloramphenicol, 30μg/ml kanamycin. For *C. crescentus*, 10μg/ml (liquid) or 50mg/ml (plate) ampicillin, 2μg/ml (liquid) or 1μg/ml (plate) chloramphenicol, 5μg/ml (liquid) or 25μg/ml (plate) kanamycin. Diaminopimelic acid (DAP) was supplemented at 300μM and sucrose at 3% w/v for conjugation and recombination methods respectively. All chemicals were purchased from Sigma-Aldrich or VWR.

Plasmid Construction:

A list of all strains, plasmids, and primers used in this study is available in Tables S1-3. Details on construction of p4B expression plasmids, pNPTS138 integration plasmids, and protein purification plasmids can be found in Supporting Information. Plasmids were introduced to *E. coli* using standard transformation techniques with chemically competent or electrocompetent cells, and to *C. crescentus* using conjugation via *E. coli* strain WM3064.

386 *Genome Engineering of* C. crescentus*:*

387 The $(GGSG)_4$-SpyTag-$(GGSG)_4$ sequence was integrated into the genomic copy of rsaA
388 using a 2-step recombination technique and sucrose counterselection. The pNPTS-
389 rsaA(SpyTag) integration plasmids were conjugated into *C. crescentus CB15NΔsap* and plated
390 on PYE with kanamycin to select for integration of the plasmid. Successful integrants were
391 incubated in liquid media overnight and plated on PYE supplemented with 3% (*w/v*) sucrose to
392 select for excision of the plasmid and *sacB* gene, leaving the SpyTag sequence behind.
393 Colonies were then spotted on PYE with kanamycin plates to confirm loss of plasmid-borne
394 kanamycin gene. Integration of the SpyTag sequence and removal of the *sacB* gene was
395 confirmed by colony PCR with OneTaq Hot Start Quick-Load 2x Master Mix with GC buffer
396 (New England BioLabs) using a Touchdown thermocycling protocol with an annealing
397 temperature ranging from 72°-62°C, decreasing 1° per cycle.

398 Successful RsaA-SpyTag protein expression was confirmed by band shift in whole cell
399 lysate in Laemmli buffer and 0.05% 2-mercaptoethanol on a BioRad Criterion Stain-free 4-20%
400 SDS-PAGE. The gel was UV-activated for 5 minutes before imaging on a ProteinSimple
401 FluorChem E system. As RsaA was migrating higher than expected, western blot was
402 performed for confirmation. A Bio-Rad Trans-Blot Turbo system with nitrocellulose membrane
403 was used to transfer protein from the SDS-PAGE gel and the membrane incubated in Thermo-
404 Fisher SuperBlock buffer for 1 hr. The protein of interest was first labeled during a 30 min
405 incubation with Rabbit-C Terminal Anti-RsaA polyclonal antibody[58] (Courtesy of the Smit lab.
406 1:5000 in TBST, Tris-Buffered Saline with 0.1-0.05% Tween-20), followed by another 30 min
407 incubation with Goat-Anti Rabbit-HRP (Sigma-Aldrich. 1:5000 in TBST). BioRad Precision Plus
408 Protein Standards (Bio-Rad) were labeled with Precision Protein StrepTactin-HRP conjugate
409 antibodies (Bio-Rad. 1:5000 in TBST). HRP fluorescence was activated with Thermo-Fisher
410 SuperSignal West Pico Chemiluminescent Substrate and imaged in chemiluminescent mode.
411 TBST washes were performed between each incubation step. The relative molecular weight of

412 bands quantified against the BioRad Precision Plus Protein Standards using ProteinSimple's
413 AlphaView software.
414
415 *Monitoring Ligation of SpyCatcher-fusions to* C. crescentus*:*
416 For flow cytometry experiments, cells were grown at 25°C to mid-log phase and cells
417 containing the pBXMCS-2-RFP plasmid were induced for 1-2 hours with 0.03% xylose to serve
418 as a positive control. A population of ~10^8 cells (determined by optical density measurement
419 where OD_{600} of 0.05 contains 10^8 cells) were harvested by centrifugation at 8,000 RCF for 5-10
420 minutes and resuspended in PBS+0.5mM $CaCl_2$. Using the cell density as determined by OD_{600}
421 and assuming assuming 4.5×10^4 RsaA monomers/cell[33], we added SpyCatcher-mRPF1 to a
422 final molar ratio of 1:20 - RsaA protein to SpyCatcher-mRFP1 . The reaction was then incubated
423 for 1 hour at room temperature with rotation. All samples were protected from light with
424 aluminum foil during the procedure and washed twice with 1ml of PBS+0.5mM $CaCl_2$ buffer prior
425 to imaging to remove any unbound protein. Cells were diluted to 10^6 cells/ml and analyzed on a
426 BD LSR Fortessa. Data on forward scatter (area and height), side scatter, and PE Texas Red
427 (561mm laser, 600 LP 610/20 filter) was collected. A total of 150,000 events for each strain was
428 measured over three experiments.
429 For each strain, the total population was gated using scatter measurements to remove
430 events corresponding to aggregates and debris. All events from the resulting main population
431 were used to create histograms of the fluorescence intensity of bound SpyCatcher-mRPF1 for
432 each strain expressing RsaA (wild-type control) or RsaA-SpyTag (Figure 4A). These
433 fluorescence intensity values were also used to calculate the absolute intensity of bound of
434 SpyCatcher-mRFP1 for RsaA-SpyTag insertion location (I_{loc}) shown in Table 1. The relative
435 SpyCatcher-mRFP1 binding ($I_{loc,rel}$) was calculated by normalizing (I_{loc}) by the absolute intensity
436 at location 467:

$$I_{loc,rel} = \frac{I_{loc}}{I_{467}} \quad \text{Eqn. 1}$$

For confocal microscopy, cells were grown to mid-log phase and ~10^8 cells (again determined by OD_{600} measurement) harvested by centrifugation at 8,000 RCF for 5-10 minutes. They were then resuspended in PBS+0.5mM $CaCl_2$ and, as in the flow cytometry experiments, a 1:20 ratio of RsaA protein to fluorescent probe, i.e. mRFP1, SpyCatcher-mRFP1, SpyCatcher-ELP-mCherry, or ELP-mCherry was added. The reaction was then incubated for 1 hour at room temperature with rotation for the mRFP1 probes and 24 hours at 4°C for the ELP-mCherry probes. 2x10^7 cells were incubated with 100nM QDs for 24 hours at 4°C with rotation. All samples were protected from light with aluminum foil during the procedure and washed twice with 1ml of buffer prior to imaging to remove any unbound protein. After the wash, cells with fluorescent probes were stained with 1μM of DAPI ((4',6-diamidino-2-phenylindole). All samples were spotted onto agarose pads (1.5% *w/v* agarose in distilled water) and mounted between glass slides and glass coverslips. Immersol 518F immersion oil with a refractive index of 1.518 was placed between the sample and the 100x oil immersion objective (Plan-Apochromat, 1.40 NA) prior to imaging. Fluorescence and IRM images were collected using a Zeiss LSM 710 confocal microscope (Carl Zeiss Micro Imaging, Thornwood, NY) with the Zen Black software. For fluorescent imaging, a 561nm laser was used for RFP/mCherry excitation and 405nm for DAPI. For IRM, a 514nm laser was reflected into the sample using a mBST80/R20 plate, then the reflected light collected and imaged onto the detector. Images were false colored and brightness/contrast adjusted using ImageJ[59].

To quantify the binding of SpyCatcher-mRFP1 to RsaA-SpyTag, the same procedure was used as above except with a 1:2 ratio of RsaA to RFP was used and incubation for 24 hours at 4°C with rotation. The reaction was visualized on a BioRad Criterion Stain-free 7.5% SDS-PAGE in Laemmli buffer with 0.05% 2-mercaptoethanol and the molecular weight of bands quantified against BioRad Precision Plus Protein Standards using Protein Simple's AlphaView

462 software.). The measurements were made in triplicate on two separate occasions and all six
463 results averaged for the final percentage reported. For each experiment, the density of bands
464 was measured using ImageJ[59]. Background subtraction was applied to the entire image and the
465 background-subtracted integrated density within an equal area was determined for each RsaA-
466 SpyTag protein band. The integrated density of the bands from triplicate reactions lacking
467 SpyCatcher were averaged to give $I_{unreact}$. To calculate the percentage of $RsaA_{467}$:SpyTag
468 ligated to SpyCatcher-mRFP1 for each experiment, we calculated the difference in density
469 between each RsaA-SpyTag band from reactions with SpyCatcher-mRFP1 ($I_{react,1}$, $I_{react,2}$, $I_{react,3}$)
470 relative to the unreacted control ($I_{unreact}$) and normalized this value by the unreacted control
471 ($I_{unreact}$):

472 $$P_{467} = \frac{1}{3}\sum_{i=1}^{3}\frac{I_{unreact}-I_{react,i}}{I_{unreact}} \qquad \text{Eqn. 2}$$

473 The reported value (P_{467}) is an average of the two experiments. We then used the absolute
474 percentage of ligation at location 467 (P_{467}) and the relative binding of SpyCatcher-mRFP1 at
475 each location to calculate the percentage of ligation for all the insertion positions.

476 $$P_{loc} = I_{loc,rel}\times P_{467} \qquad \text{Eqn. 3}$$

477 The values of P_{loc} are shown in Table 1.

478

479 *Cell viability assay:*
480
481 Cell viability in the presence of SpyCatcher-QDs was determined using the viable plate
482 count method. Approximately $4x10^8$ mid-log phase cells (day 0) (cell number determined by
483 OD_{600} measurement) were first incubated with 100nM SpyCatcher-QDs in M2G buffer (1X M2
484 salts without NH_4Cl to prevent extensive cell growth, 1mM $MgSO_4$, 0.5mM $CaCl_2$, 2% glucose)
485 for 24 hours at 4°C with rotation to allow QD ligation to the cell surface. Post-binding (day 1), the
486 cultures were transferred to a 25°C humidified incubator and left stationary for two weeks.
487 Cultures were sampled at different time points (days 2, 7, and 14), serially diluted, and titered on

PYE agar plates (0.2% peptone, 0.1% yeast extract, 1mM $MgSO_4$, 0.5mM $CaCl_2$, 1.5% agar), which were incubated at 30°C for two days. Colonies on the plates were counted and cell viability was quantified by enumeration of Colony Forming Units/mL as follows:

CFU/mL = Number of colonies / Dilution x Volume plated (mL)

At the specified time points, 30µl of culture was removed from the tube and centrifuged at 16,000 x g for 1 minute. The supernatant was discarded and the cells were resuspended in 3µl M2G buffer. A 1.5% agarose pad was prepared on a 25x75mm glass slide and 0.6µl of the resuspended culture was placed on it. An 18x18mm coverslip was then placed on the pad, and the trapped cells were imaged and processed using as outlined above.

In situ atomic force microscope (AFM) imaging:

Mid-log cultures of *C. crescentus* JS4038 carrying p4B-rsaA_{600}, p4B-rsaA_{600}690: $(GGSG)_4$-spytag-$(GGSG)_4$, or p4B-rsaA_{600}690: $(GGSG)_4$-spytag-$(GGSG)_4$, were harvested at 8000 rpm for 5 minutes and the pellet resuspended in PBS + 5mM $CaCl_2$ buffer. The JS4038 strain is defective in capsular polysaccharide synthesis. This is necessary for AFM imaging as the the capsular polysaccharide layer obscures the S-layer lattice. The cells were washed three times to remove any debris. 100µL of the washed cell culture was applied to a poly-L-lysine coated glass coverslip (12mm cover glasses, BioCoat from VWR) which was pre-mounted onto a metal puck. The sample was incubated at room temperature for 1 hr to allow sufficient cell attachment and then 1mL of PBS + 5mM $CaCl_2$ buffer was used to wash away unbound cells from the glass surface. 50µL of PBS + 5mM $CaCl_2$ buffer was added to the resulting glass surface, and the sample was transferred onto the sample stage for imaging.

In situ AFM imaging was performed on a Bruker Multimode AFM using PeakForce Tapping mode in liquid. An Olympus Biolever-mini cantilever (BL-AC40TS) was used for high resolution imaging. The following set of parameters was normally employed to ensure the best

image quality: 0.2 to 0.5Hz scanning rate, 512 × 512 scanning lines, 15nm peak force amplitude, and 50 to 100 pN peak force setpoint.

Further methods on plasmid construction, protein purification, and QD synthesis can be found in Supporting Information.

Supporting Information Description

Abbreviations

4',6-diamidino-2-phenylindole (DAPI); Elastin-like polypeptide (ELP); Engineered Living Material (ELM); Quantum dot (QD); Red fluorescent protein (RFP); Surface-layer (S-layer) S-layer associated protease (sapA); Atomic force microscopy (AFM); Interference reflectance microscopy (IRM); SpyTag (ST); SpyCatcher (SC).

Author Information:

Acknowledgement:

We are indebted to Prof. John Smit and Dr. John Nomellini for helpful conversations and starting materials. We also thank Dr. Francesca Manea for her contributions to the S-layer research at the Molecular Foundry and Dr. Andrew Hagen for the gift of the pARH356 plasmid. This work was supported by the Defense Advanced Research Projects Agency (Engineered Living Materials Program, C.M.A-F.) and National Institutes of Health award R01NS096317 (B.E.C.) Work at the Molecular Foundry was supported by the Office of Science, Office of Basic Energy Sciences, of the U.S. Department of Energy under Contract No. DE-AC02-05CH11231.

References

(1) Mann, S. *Biomineralization: Principles and Concepts in Bioinorganic Materials Chemistry*;

Oxford University Press, 2001.
(2) Chen, A. Y.; Zhong, C.; Lu, T. K. Engineering Living Functional Materials. *ACS Synth. Biol.* **2015**, *4* (1), 8–11.
(3) Nguyen, P. Q.; Courchesne, N.-M. D.; Duraj-Thatte, A.; Praveschotinunt, P.; Joshi, N. S. Engineered Living Materials: Prospects and Challenges for Using Biological Systems to Direct the Assembly of Smart Materials. *Adv. Mater.* **2018**, *30* (19), e1704847.
(4) Chen, A. Y.; Deng, Z.; Billings, A. N.; Seker, U. O. S.; Lu, M. Y.; Citorik, R. J.; Zakeri, B.; Lu, T. K. Synthesis and Patterning of Tunable Multiscale Materials with Engineered Cells. *Nat. Mater.* **2014**, *13*, 515.
(5) Zhou, A. Y.; Baruch, M.; Ajo-Franklin, C. M.; Maharbiz, M. M. A Portable Bioelectronic Sensing System (BESSY) for Environmental Deployment Incorporating Differential Microbial Sensing in Miniaturized Reactors. *PLoS One* **2017**, *12* (9), e0184994.
(6) Gerber, L. C.; Koehler, F. M.; Grass, R. N.; Stark, W. J. Incorporating Microorganisms into Polymer Layers Provides Bioinspired Functional Living Materials. *Proc. Natl. Acad. Sci. U. S. A.* **2012**, *109* (1), 90–94.
(7) Lee, S. Y.; Choi, J. H.; Xu, Z. Microbial Cell-Surface Display. *Trends Biotechnol.* **2003**, *21* (1), 45–52.
(8) Nussbaumer, M. G.; Nguyen, P. Q.; Tay, P. K. R.; Naydich, A.; Hysi, E.; Botyanszki, Z.; Joshi, N. S. Bootstrapped Biocatalysis: Biofilm-Derived Materials as Reversibly Functionalizable Multienzyme Surfaces. *ChemCatChem* **2017**, *9* (23), 4328–4333.
(9) Nguyen, P. Q.; Botyanszki, Z.; Tay, P. K. R.; Joshi, N. S. Programmable Biofilm-Based Materials from Engineered Curli Nanofibres. *Nat. Commun.* **2014**, *5*, 4945.
(10) Seker, U. O. S.; Chen, A. Y.; Citorik, R. J.; Lu, T. K. Synthetic Biogenesis of Bacterial Amyloid Nanomaterials with Tunable Inorganic–Organic Interfaces and Electrical Conductivity. *ACS Synth. Biol.* **2017**, *6* (2), 266–275.
(11) Zhong, C.; Gurry, T.; Cheng, A. A.; Downey, J.; Deng, Z.; Stultz, C. M.; Lu, T. K. Strong Underwater Adhesives Made by Self-Assembling Multi-Protein Nanofibres. *Nat. Nanotechnol.* **2014**, *9*, 858.
(12) Nicolay, T.; Vanderleyden, J.; Spaepen, S. Autotransporter-Based Cell Surface Display in Gram-Negative Bacteria. *Crit. Rev. Microbiol.* **2015**, *41* (1), 109–123.
(13) Daugherty, P. S. Protein Engineering with Bacterial Display. *Curr. Opin. Struct. Biol.* **2007**, *17* (4), 474–480.
(14) Messner, P.; Schäffer, C.; Egelseer, E.-M.; Sleytr, U. B. Occurrence, Structure, Chemistry, Genetics, Morphogenesis, and Functions of S-Layers. In *Prokaryotic Cell Wall Compounds: Structure and Biochemistry*; König, H., Claus, H., Varma, A., Eds.; Springer Berlin Heidelberg: Berlin, Heidelberg, 2010; pp 53–109.
(15) Roberts, K.; Grief, C.; Hills, G. J.; Shaw, P. J. Cell Wall Glycoproteins: Structure and Function. *J. Cell Sci. Suppl.* **1985**, *2*, 105–127.
(16) Lembcke, G.; Baumeister, W.; Beckmann, E.; Zemlin, F. Cryo-Electron Microscopy of the Surface Protein of Sulfolobus Shibatae. *Ultramicroscopy* **1993**, *49* (1), 397–406.
(17) Smit, J.; Engelhardt, H.; Volker, S.; Smith, S. H.; Baumeister, W. The S-Layer of Caulobacter Crescentus: Three-Dimensional Image Reconstruction and Structure Analysis by Electron Microscopy. *J. Bacteriol.* **1992**, *174* (20), 6527–6538.
(18) Baranova, E.; Fronzes, R.; Garcia-Pino, A.; Van Gerven, N.; Papapostolou, D.; Péhau-Arnaudet, G.; Pardon, E.; Steyaert, J.; Howorka, S.; Remaut, H. SbsB Structure and Lattice Reconstruction Unveil Ca2+ Triggered S-Layer Assembly. *Nature* **2012**, *487* (7405), 119–122.
(19) Messner, P.; Pum, D.; Sleytr, U. B. Characterization of the Ultrastructure and the Self-Assembly of the Surface Layer of Bacillus Stearothermophilus Strain NRS 2004/3a. *J. Ultrastruct. Mol. Struct. Res.* **1986**, *97* (1-3), 73–88.
(20) Norville, J. E.; Kelly, D. F.; Knight, T. F., Jr; Belcher, A. M.; Walz, T. 7A Projection Map

of the S-Layer Protein sbpA Obtained with Trehalose-Embedded Monolayer Crystals. *J. Struct. Biol.* **2007**, *160* (3), 313–323.
(21) Wildhaber, I.; Baumeister, W. The Cell Envelope of Thermoproteus Tenax: Three-Dimensional Structure of the Surface Layer and Its Role in Shape Maintenance. *EMBO J.* **1987**, *6* (5), 1475–1480.
(22) Pum, D.; Messner, P.; Sleytr, U. B. Role of the S Layer in Morphogenesis and Cell Division of the Archaebacterium Methanocorpusculum Sinense. *J. Bacteriol.* **1991**, *173* (21), 6865–6873.
(23) Kern, J.; Schneewind, O. BslA, the S-Layer Adhesin of B. Anthracis, Is a Virulence Factor for Anthrax Pathogenesis. *Mol. Microbiol.* **2010**, *75* (2), 324–332.
(24) Koval, S. F.; Hynes, S. H. Effect of Paracrystalline Protein Surface Layers on Predation by Bdellovibrio Bacteriovorus. *J. Bacteriol.* **1991**, *173* (7), 2244–2249.
(25) Åvall-Jääskeläinen, S.; Lindholm, A.; Palva, A. Surface Display of the Receptor-Binding Region of the Lactobacillus Brevis S-Layer Protein in Lactococcus Lactis Provides Nonadhesive Lactococci with the Ability to Adhere to Intestinal Epithelial Cells. *Appl. Environ. Microbiol.* **2003**, *69* (4), 2230–2236.
(26) Sleytr, U. B.; Schuster, B.; Egelseer, E.-M.; Pum, D. S-Layers: Principles and Applications. *FEMS Microbiol. Rev.* **2014**, *38* (5), 823–864.
(27) Ilk, N.; Egelseer, E. M.; Sleytr, U. B. S-Layer Fusion Proteins—construction Principles and Applications. *Curr. Opin. Biotechnol.* **2011**, *22* (6), 824–831.
(28) Patel, J.; Zhang, Q.; McKay, R. M. L.; Vincent, R.; Xu, Z. Genetic Engineering of Caulobacter Crescentus for Removal of Cadmium from Water. *Appl. Biochem. Biotechnol.* **2010**, *160* (1), 232–243.
(29) Farr, C.; Nomellini, J. F.; Ailon, E.; Shanina, I.; Sangsari, S.; Cavacini, L. A.; Smit, J.; Horwitz, M. S. Development of an HIV-1 Microbicide Based on Caulobacter Crescentus: Blocking Infection by High-Density Display of Virus Entry Inhibitors. *PLoS One* **2013**, *8* (6), e65965.
(30) Bharat, T. A. M.; Kureisaite-Ciziene, D.; Hardy, G. G.; Yu, E. W.; Devant, J. M.; Hagen, W. J. H.; Brun, Y. V.; Briggs, J. A. G.; Löwe, J. Structure of the Hexagonal Surface Layer on Caulobacter Crescentus Cells. *Nat Microbiol* **2017**, *2*, 17059.
(31) Laub, M. T.; Shapiro, L.; McAdams, H. H. Systems Biology of Caulobacter. *Annu. Rev. Genet.* **2007**, *41*, 429–441.
(32) Crosson, S.; McGrath, P. T.; Stephens, C.; McAdams, H. H.; Shapiro, L. Conserved Modular Design of an Oxygen Sensory/signaling Network with Species-Specific Output. *Proc. Natl. Acad. Sci. U. S. A.* **2005**, *102* (22), 8018–8023.
(33) Amat, F.; Comolli, L. R.; Nomellini, J. F.; Moussavi, F.; Downing, K. H.; Smit, J.; Horowitz, M. Analysis of the Intact Surface Layer of Caulobacter Crescentus by Cryo-Electron Tomography. *J. Bacteriol.* **2010**, *192* (22), 5855–5865.
(34) Bingle, W. H.; Nomellini, J. F.; Smit, J. Cell-Surface Display of a Pseudomonas Aeruginosa Strain K Pilin Peptide within the Paracrystalline S-Layer of Caulobacter Crescentus. *Mol. Microbiol.* **1997**, *26* (2), 277–288.
(35) Park, D. M.; Reed, D. W.; Yung, M. C.; Eslamimanesh, A.; Lencka, M. M.; Anderko, A.; Fujita, Y.; Riman, R. E.; Navrotsky, A.; Jiao, Y. Bioadsorption of Rare Earth Elements through Cell Surface Display of Lanthanide Binding Tags. *Environ. Sci. Technol.* **2016**, *50* (5), 2735–2742.
(36) Gandham, L.; Nomellini, J. F.; Smit, J. Evaluating Secretion and Surface Attachment of SapA, an S-Layer-Associated Metalloprotease of Caulobacter Crescentus. *Arch. Microbiol.* **2012**, *194* (10), 865–877.
(37) Zakeri, B.; Fierer, J. O.; Celik, E.; Chittock, E. C.; Schwarz-Linek, U.; Moy, V. T.; Howarth, M. Peptide Tag Forming a Rapid Covalent Bond to a Protein, through Engineering a Bacterial Adhesin. *Proc. Natl. Acad. Sci. U. S. A.* **2012**, *109* (12), E690–E697.

(38) Reddington, S. C.; Howarth, M. Secrets of a Covalent Interaction for Biomaterials and Biotechnology: SpyTag and SpyCatcher. *Curr. Opin. Chem. Biol.* **2015**, *29*, 94–99.
(39) Lau, J. H. Y.; Nomellini, J. F.; Smit, J. Analysis of High-Level S-Layer Protein Secretion in Caulobacter Crescentus. *Can. J. Microbiol.* **2010**, *56* (6), 501–514.
(40) Nomellini, J. F.; Duncan, G.; Dorocicz, I. R.; Smit, J. S-Layer-Mediated Display of the Immunoglobulin G-Binding Domain of Streptococcal Protein G on the Surface of Caulobacter Crescentus: Development of an Immunoactive Reagent. *Appl. Environ. Microbiol.* **2007**, *73* (10), 3245–3253.
(41) Hagen, A.; Sutter, M.; Sloan, N.; Kerfeld, C. A. Programmed Loading and Rapid Purification of Engineered Bacterial Microcompartment Shells. *Nat. Commun.* **2018**, *9* (1), 2881.
(42) Bedbrook, C. N.; Kato, M.; Ravindra Kumar, S.; Lakshmanan, A.; Nath, R. D.; Sun, F.; Sternberg, P. W.; Arnold, F. H.; Gradinaru, V. Genetically Encoded Spy Peptide Fusion System to Detect Plasma Membrane-Localized Proteins In Vivo. *Chem. Biol.* **2015**, *22* (8), 1108–1121.
(43) Campbell, R. E.; Tour, O.; Palmer, A. E.; Steinbach, P. A.; Baird, G. S.; Zacharias, D. A.; Tsien, R. Y. A Monomeric Red Fluorescent Protein. *Proc. Natl. Acad. Sci. U. S. A.* **2002**, *99* (12), 7877–7882.
(44) Muiznieks, L. D.; Reichheld, S. E.; Sitarz, E. E.; Miao, M.; Keeley, F. W. Proline-Poor Hydrophobic Domains Modulate the Assembly and Material Properties of Polymeric Elastin: Role of Domain 30 in Elastin Assembly and Material Properties. *Biopolymers* **2015**, *103* (10), 563–573.
(45) Sun, F.; Zhang, W.-B.; Mahdavi, A.; Arnold, F. H.; Tirrell, D. A. Synthesis of Bioactive Protein Hydrogels by Genetically Encoded SpyTag-SpyCatcher Chemistry. *Proceedings of the National Academy of Sciences* **2014**, *111* (31), 11269–11274.
(46) Wichner, S. M.; Mann, V. R.; Powers, A. S.; Segal, M. A.; Mir, M.; Bandaria, J. N.; DeWitt, M. A.; Darzacq, X.; Yildiz, A.; Cohen, B. E. Covalent Protein Labeling and Improved Single-Molecule Optical Properties of Aqueous CdSe/CdS Quantum Dots. *ACS Nano* **2017**, *11* (7), 6773–6781.
(47) Mann, V. R.; Powers, A. S.; Tilley, D. C.; Sack, J. T.; Cohen, B. E. Azide-Alkyne Click Conjugation on Quantum Dots by Selective Copper Coordination. *ACS Nano* **2018**, *12* (5), 4469–4477.
(48) Sakimoto, K. K.; Wong, A. B.; Yang, P. Self-Photosensitization of Nonphotosynthetic Bacteria for Solar-to-Chemical Production. *Science* **2016**, *351* (6268), 74–77.
(49) Rothfuss, H.; Lara, J. C.; Schmid, A. K.; Lidstrom, M. E. Involvement of the S-Layer Proteins Hpi and SlpA in the Maintenance of Cell Envelope Integrity in Deinococcus Radiodurans R1. *Microbiology* **2006**, *152* (Pt 9), 2779–2787.
(50) Gerbino, E.; Carasi, P.; Mobili, P.; Serradell, M. A.; Gómez-Zavaglia, A. Role of S-Layer Proteins in Bacteria. *World J. Microbiol. Biotechnol.* **2015**, *31* (12), 1877–1887.
(51) Schultze-Lam, S.; Harauz, G.; Beveridge, T. J. Participation of a Cyanobacterial S Layer in Fine-Grain Mineral Formation. *J. Bacteriol.* **1992**, *174* (24), 7971–7981.
(52) Küpcü, S.; Mader, C.; Sára, M. The Crystalline Cell Surface Layer from Thermoanaerobacter Thermohydrosulfuricus L111-69 as an Immobilization Matrix: Influence of the Morphological Properties and the Pore Size of the Matrix on the Loss of Activity of Covalently Bound Enzymes. *Biotechnol. Appl. Biochem.* **1995**, *21* (3), 275–286.
(53) Martín, M. J.; Lara-Villoslada, F.; Ruiz, M. A.; Morales, M. E. Microencapsulation of Bacteria: A Review of Different Technologies and Their Impact on the Probiotic Effects. *Innov. Food Sci. Emerg. Technol.* **2015**, *27*, 15–25.
(54) Schoebitz, M.; López, M. D.; Roldán, A. Bioencapsulation of Microbial Inoculants for Better Soil–plant Fertilization. A Review. *Agron. Sustain. Dev.* **2013**.
(55) Herrero, M.; Stuckey, D. C. Bioaugmentation and Its Application in Wastewater

Treatment: A Review. *Chemosphere* **2015**, *140*, 119–128.
(56) Kandemir, N.; Vollmer, W.; Jakubovics, N. S.; Chen, J. Mechanical Interactions between Bacteria and Hydrogels. *Sci. Rep.* **2018**, *8* (1), 10893.
(57) Azam, A.; Tullman-Ercek, D. Type-III Secretion Filaments as Scaffolds for Inorganic Nanostructures. *J. R. Soc. Interface* **2016**, *13* (114), 20150938.
(58) Toporowski, M. C.; Nomellini, J. F.; Awram, P.; Smit, J. Two Outer Membrane Proteins Are Required for Maximal Type I Secretion of the Caulobacter Crescentus S-Layer Protein. *J. Bacteriol.* **2004**, *186* (23), 8000–8009.
(59) Schneider, C. A.; Rasband, W. S.; Eliceiri, K. W. NIH Image to ImageJ: 25 Years of Image Analysis. *Nat. Methods* **2012**, *9* (7), 671–675.
(60) Evinger, M.; Agabian, N. Envelope-Associated Nucleoid from Caulobacter Crescentus Stalked and Swarmer Cells. *J. Bacteriol.* **1977**, *132* (1), 294–301.
(61) Spratt, B. G.; Hedge, P. J.; te Heesen, S.; Edelman, A.; Broome-Smith, J. K. Kanamycin-Resistant Vectors That Are Analogues of Plasmids pUC8, pUC9, pEMBL8 and pEMBL9. *Gene* **1986**, *41* (2-3), 337–342.
(62) Thanbichler, M.; Iniesta, A. A.; Shapiro, L. A Comprehensive Set of Plasmids for Vanillate- and Xylose-Inducible Gene Expression in Caulobacter Crescentus. *Nucleic Acids Res.* **2007**, *35* (20), e137.
(63) Abudayyeh, O. O.; Gootenberg, J. S.; Konermann, S.; Joung, J.; Slaymaker, I. M.; Cox, D. B. T.; Shmakov, S.; Makarova, K. S.; Semenova, E.; Minakhin, L.; et al. C2c2 Is a Single-Component Programmable RNA-Guided RNA-Targeting CRISPR Effector. *Science* **2016**, *353* (6299), aaf5573.